Raman and infrared spectra of graphite-$AlCl_3$

G. M. Gualberto,*† C. Underhill,* S. Y. Leung,*‡ and G. Dresselhaus§
Massachusetts Institute of Technology, Cambridge, Massachusetts 02139
(Received 13 July 1979)

Raman and infrared spectra on well-staged graphite-$AlCl_3$ are reported for compounds with stages $n = 1$, 2, 4, and 8. Of significance is the absence of infrared-active modes for stage-1 graphite-$AlCl_3$ and the presence in stages 2, 4, and 8 of three infrared-active modes in the vicinity of the graphite E_{1u} mode. The Raman-active modes in graphite-$AlCl_3$ behave similarly to the corresponding bounding-layer and interior-layer graphitic modes in graphite-$FeCl_3$ with regard to the stage dependence of the peak frequencies and relative intensities.

INTRODUCTION

The lattice dynamics of highly oriented pyrolytic graphite (HOPG) have been studied by a variety of experimental techniques, such as inelastic neutron scattering,[1] Raman scattering,[2,3] and infrared spectroscopy.[4] Of the various techniques which have thus far been applied to the study of intercalation compounds, Raman and infrared spectroscopy are important techniques because they provide specific information on each type of layer plane that occurs in graphite intercalation compounds: "interior graphite" layers, "bounding graphite" layers (the graphite layers adjacent to the intercalate layers), and "intercalate" layers.[5-12] Graphitic Raman modes in the vicinity of 1600 cm^{-1} have been observed for a variety of intercalate species as doublet structures separated by approximately 20 cm^{-1}. The lower frequency $E^0_{2g_2}$ component is associated with the interior graphite layers and the upper frequency $\hat{E}_{2g_2}$ component with bounding graphite layers.[5-11] The present Raman and ir study has been carried out on well-characterized graphite-$AlCl_3$ acceptor samples. These techniques provide complementary information on the phonon spectra for these materials.

The graphite-$AlCl_3$ system is especially attractive for the study of acceptor compounds for the following reasons. Most significantly, it is possible to make well-staged samples with essentially no secondary-stage inclusions. In particular, for the $AlCl_3$ system, single-staged stage-1 compounds can be readily fabricated, in contrast with the acceptors Br_2 (where no stage-1 compound has ever been prepared[5]) and $FeCl_3$ (where sample preparation difficulties have so far precluded the fabrication of a single-staged stage-1 compound[11]). One major emphasis of the present work is an elucidation of the behavior of the Raman and infrared spectra for a good stage-1 acceptor compound. Attention is also given to the Raman and infrared spectra for single-staged, well-characterized higher-stage compounds with $AlCl_3$. Although preliminary Raman spectra were previously reported for graphite-$AlCl_3$,[13] this is the first systematic study of the Raman spectra and the first report of infrared spectra for this system.

EXPERIMENTAL

Samples were prepared using highly oriented pyrolytic graphite as a host material. The graphite specimens were cut to typical dimensions $7 \times 7 \times 0.1$ mm. Dry Cl_2 gas was passed over heated aluminum wire (99.85% purity) and $AlCl_3$ was formed in the cooler regions of the tube (see Fig. 1). The ampoule containing HOPG and the $AlCl_3$ crystallites was sealed with an atmosphere of 300 Torr of Cl_2 gas. When HOPG is employed as a host material, staging conditions are somewhat different with respect to those for single crystal or flake graphite.[14-16] However, consistent with previously reported results for alkali metal (Ref. 8), $FeCl_3$ (Ref. 11), and halogen (Ref. 17) intercalants, it is possible to produce a series of well-staged, homogeneous crystals over a wide range of intercalate concentrations using the conventional two-zone growth technique.[18,19] In this way, single-staged samples were prepared for stages $n = 1$, 2, 4, and 8. For the growth process employed, the graphite temperature was maintained at 286° C and the $AlCl_3$ temperature at 235°C. Varying amounts of $AlCl_3$ were condensed into the ampoules, such that with excess $AlCl_3$ a stage-1 compound resulted. For dilute samples, the quantity of $AlCl_3$ was reduced such that at the conclusion of the reaction no visible signs of the intercalant remained in the ampoule. In this way single-staged compounds with $n = 2$, 4, and 8 were produced. This growth procedure is different from that used by Rüdorff and Zeller[20] to obtain graphite-$AlCl_3$ compounds of stages 1, 2, and 4.

The stage for each sample was determined by

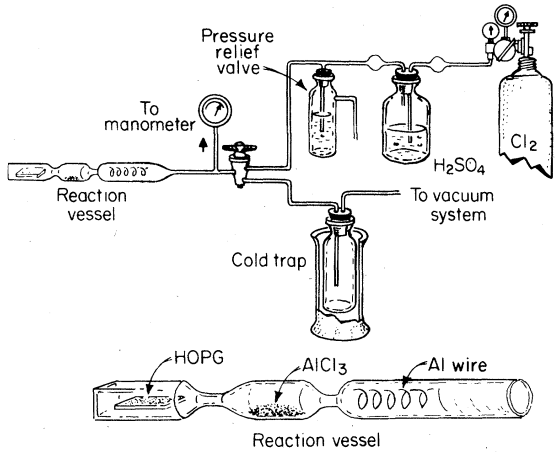

FIG. 1. Schematic diagram of arrangement for the preparation of graphite-$AlCl_3$ compounds. The upper portion shows the overall system while the lower portion shows the reaction vessel in more detail.

measuring the (00l) x-ray diffraction peaks from a conventional θ–2θ scan. Owing to the instability of the graphite-$AlCl_3$ compounds in air, the samples were encapsulated in square Pyrex ampoules, with wall thickness 0.7 mm. High-stage compounds (e.g., $n=8$) are relatively stable and can be stored in methanol. The samples were positioned in the diffractometer to maximize the diffracted intensity using a goniometer which allowed both translational and rotational degrees of freedom. Mo $K\alpha$ radiation was selected to obtain x-ray penetration of the glass; only about 25% of the incident intensity was transmitted through 1.4 mm of glass (twice the wall thickness). A Si(Li) detector and a single channel analyzer were used to provide discrimination of the incident x-ray energy. The presence of admixed stages could be detected from the observation of (00l) lines characteristic of mixed phases. The good sample quality with regard to the absence of admixed secondary phases is demonstrated by Fig. 2, where the diffractometer scans for the samples reported in this work are presented. Also shown in the figure are values for the corresponding intercalant repeat distances I_c. It is interesting to note that integrated intensity measurements for the (00l) diffraction peaks are in qualitative agreement with those calculated for a sandwich intercalant.[21,22] In particular, a maximum peak intensity is observed for the (003), (006), and (009) lines for stage $n=1$, corresponding to the (0 0 $(n+2)p$) lines where p is an integer. However, for higher 2θ values, deviations from the above sequence are observed; for example, the (0 0 11) line is more intense than the (0 0 12) line for stage-1 $AlCl_3$. This discrepancy is due to the phase factor introduced by scattering from a sandwich intercalant. A qualitatively similar agreement between the calculated peak intensity and the experimental observations for this sandwich intercalant is obtained for stages 2, 4, and 8.

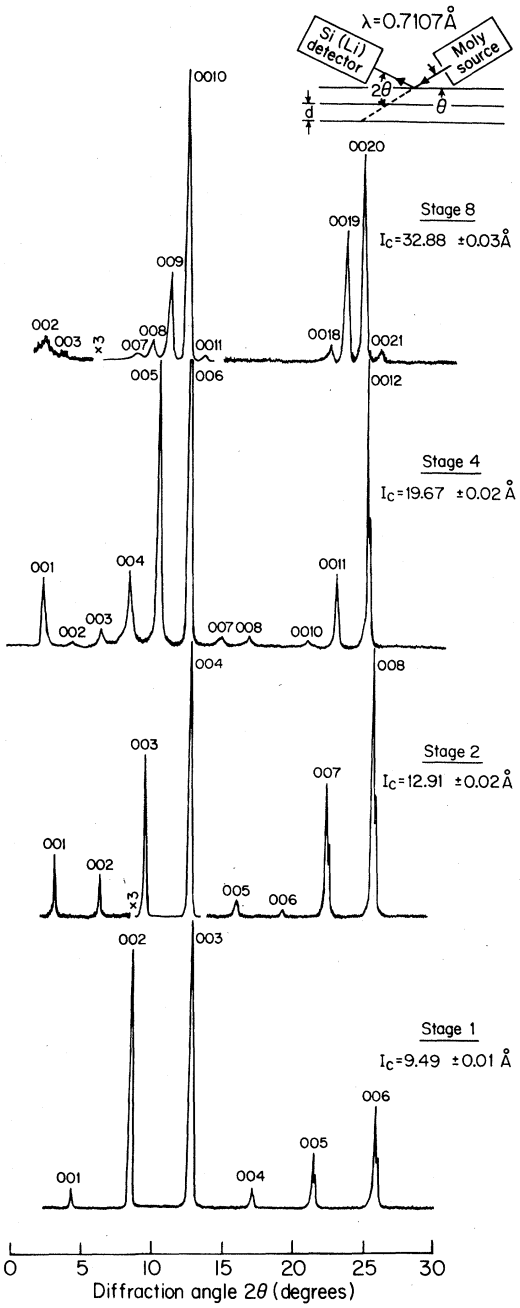

FIG. 2. Stage characterization using x-ray diffraction for stages $n=1$, 2, 4, and 8 graphite-$AlCl_3$. For each diffractogram the (0 0 l) reflections are labeled and the intercalant repeat distance I_c and stage indices are given on the right. The diffractograms were taken with a Mo x-ray source and the Si(Li) detector.

In Table I are listed the observed and calculated

TABLE I. Experimental and calculated x-ray data [a] for (00l) reflections.

	Stage 1 $I_c = 9.49 \pm 0.01$ Å					Stage 2 $I_c = 12.91 \pm 0.02$ Å			
00l	$2\theta_{exp}$ [b]	$2\theta_{cal}$	I_{exp}	I_{cal}	00l	$2\theta_{exp}$ [c]	$2\theta_{cal}$	I_{exp}	I_{cal}
0 0 1	4.30	4.29	270	351	0 0 1	3.39	3.15	481	2 252
0 0 2	8.62	8.59	1 192	4 363	0 0 2	6.24	6.31	372	539
0 0 3	13.00	12.90	10 774	9 411	0 0 3	9.40	9.47	5 037	5 178
0 0 4	17.18	17.23	497	250	0 0 4	12.59	12.64	11 829	11 868
0 0 5	21.57	21.59	1 662	110	0 0 5	15.78	15.82	176	170
0 0 6	25.98	25.97	3 354	3 070	0 0 6	18.99	19.01	22	0
0 0 8	34.88	34.87	392	386	0 0 7	22.15	22.21	1 988	631
0 0 9	39.40	39.40	603	481	0 0 8	25.45	25.44	4 283	2 533
0 0 11	48.66	48.66	132	76	0 0 11	35.31	35.25	736	730
0 0 12	53.44	53.42	98	401					

	Stage 4 $I_c = 19.67 \pm 0.02$ Å					Stage 8 $I_c = 32.88 \pm 0.03$ Å			
00l	$2\theta_{exp}$ [d]	$2\theta_{cal}$	I_{exp}	I_{cal}	00l	$2\theta_{exp}$ [e]	$2\theta_{cal}$	I_{exp}	I_{cal}
0 0 1	2.16	2.07	1 151	4 064	0 0 2	2.33	2.48	577	615
0 0 2	4.10	4.14	125	458	0 0 7	9.76	8.68	···	399
0 0 3	6.20	6.22	434	70	0 0 8	9.98	9.92	1 453	817
0 0 4	8.25	8.29	2 138	921	0 0 9	11.27	11.16	4 623	2 385
0 0 5	10.34	10.37	6 195	2 537	0 0 10	12.45	12.41	16 545	16 903
0 0 6	12.43	12.45	10 620	10 614	0 0 11	13.70	13.65	214	46
0 0 7	14.60	14.53	162	103	0 0 18	22.48	22.43	250	62
0 0 8	16.61	16.62	86	78	0 0 19	23.77	23.70	2 191	703
0 0 10	20.80	20.82	60	50	0 0 20	24.95	24.96	3 618	2 405
0 0 11	22.89	22.93	1 047	456	0 0 21	26.20	26.23	189	168
0 0 12	25.04	25.05	2 517	1 829	0 0 29	36.53	36.53	512	524
0 0 17	35.77	35.78	236	351	0 0 30	37.77	37.83	272	364
0 0 18	38.03	37.96	358	325	0 0 39	49.82	49.85	65	298

[a] The experimental intensity I_{exp} is in units counts/peak. The calculated intensity I_{cal} is scaled to the experimental values with a scale factor obtained by least-squares fitting I_{cal} to I_{exp} for all peaks.

[b] Corrected for calibration error of −0.68°.

[c] Corrected for calibration error of −0.11°.

[d] Corrected for calibration error of +0.92°.

[e] Corrected for calibration error of +0.23°.

values for 2θ and for the integrated line intensities corresponding to a variety of (00l) reflections for stage 1, 2, 4, and 8 compounds. Although the experimental errors in the data are considerable, the intensity calculation does show that the intercalate is composed of the three constituent layers: Cl_3-Al_2-Cl_3 (i.e., the Cl^- ions lie in planes adjacent to the graphite bounding layers).[22]

Room-temperature Raman spectra were obtained in the backscattering geometry using unpolarized incident light with the electric vector and the sample c axis in the scattering plane, thereby exciting in-plane Raman-active modes. To avoid intercalate desorption effects associated with laser heating, these spectra were taken at low laser power levels ($\lesssim 50$ mW) levels. Laser excitation was provided by an argon-ion laser operating at 4880 Å. The scattered radiation was analyzed by a Spex double monochromator and detected by a cooled photomultiplier. Conventional dc techniques were used for signal processing. Raman spectra were obtained with the samples enclosed in Pyrex ampoules to avoid intercalate desorption, which is very rapid for stage-1 compounds.

Infrared reflectivity spectra were obtained using a Fourier transform spectrophotometer operating with a globar source and a Triglycine-sulfate (TGS) detector with a KBr window. Room temperature spectra, covering the energy range 800 $cm^{-1} < \omega < 4000$ cm^{-1} with a resolution of 2 cm^{-1} were taken with the c axis approximately parallel to the beam path. The spectrophotometer was purged with an atmosphere of dried air and no appreciable spectral interference from water vapor absorption lines was detected in the frequency region of interest. The infrared spectra were taken on samples encapsulated in a specially built ir ampoule containing a ZnSe window. Sample mounting and transfer for the ir measurements were done in a dry box.

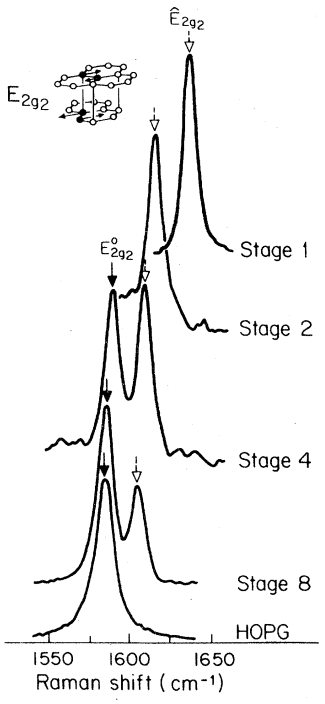

FIG. 3. Unpolarized, room temperature Raman spectra taken in the backscattering geometry ($\vec{E} \perp \vec{c}$) for HOPG and for graphite-$AlCl_3$ stages $n = 1$, 2, 4, and 8. The in-plane Raman-active E_{2g_2} graphite modes are shown in the inset. The upper frequency $\hat{E}_{2g_2}$ mode is identified with the bounding layers and the lower frequency $E^0_{2g_2}$ mode with the interior graphite layers.

RESULTS AND DISCUSSION

Raman spectra for graphite-$AlCl_3$ are shown in Fig. 3 for essentially single-staged $n = 1$, 2, 4, and 8. Also included for comparison is the spectrum for pristine graphite HOPG, showing a single line at the E_{2g_2} mode frequency (see inset). Samples for stages $n = 4$ and $n = 8$ exhibit two modes, the lower frequency $E^0_{2g_2}$ mode associated with interior graphite layers, and the upper frequency $\hat{E}_{2g_2}$ mode associated with the graphite bounding layers, consistent with previous Raman studies.[5-11] For stage $n = 4$, where the number of bounding and interior layers is equal, the two peaks have approximately equal intensity. For stage $n = 8$, where there are two bounding layers and six interior layers, the intensity for the $E^0_{2g_2}$ mode is greater than that for the $\hat{E}_{2g_2}$ mode. With increasing intercalate concentration ($1/n$), the doublet separation for stages $n = 4$ and 8 remains constant (~20 cm^{-1}) while the relative intensity of the $\hat{E}_{2g_2}$ feature increases relative to that for the $E^0_{2g_2}$ mode, in qualitative agreement with previous work on other intercalate species.[8,9,11] The spectra for stage $n = 1$ and $n = 2$ samples show only a single ($\hat{E}_{2g_2}$) line, consistent with the absence of interior graphite layers for these stages. A large intercalate concentration-dependent frequency upshift of the $\hat{E}_{2g_2}$ bounding layer mode is observed. This upshift becomes more pronounced with increasing $1/n$, and has a somewhat larger magnitude than the upshift reported for the Br_2 and $FeCl_3$ intercalants.[11,23] The spectra for stages $n = 1$ and $n = 2$ in Fig. 3 have been fit with a Lorentzian line and for stages $n = 4$ and 8, with two Lorentzian lines. The peak frequencies, intensities, and linewidths were obtained by a convolution of the Lorentzian lines with the measured instrument function and the results for the peak frequency, linewidth, and peak relative intensity are given in Table II.

Infrared reflectivity spectra for stages $n = 2$, 4, and 8 compounds and for HOPG are shown in Fig. 4. The spectrum for HOPG shows a single line at the E_{1u} mode frequency, consistent with previous work.[4]

It is of interest that infrared structure is found for the stage 2, 4, and 8 compounds, but not for the stage $n = 1$ compound. In contrast, stage-1 graphite-$AlCl_3$ does show a Raman-active mode

TABLE II. Parameters for Raman-active modes in graphite-$AlCl_3$.

Stage	Graphite interior layer ω_0 (cm^{-1}) [a]	Γ (cm^{-1}) [b]	F_R [c]	Graphite bounding layer ω_0 (cm^{-1}) [a]	Γ (cm^{-1}) [b]	F_R [c]
1	...	...	...	1635.0	3.0	1.0
2	...	...	...	1616.5	4.5	1.0
4	1588.0	5.5	1.0	1607.8	5.5	1.0
8	1584.5	6.0	2.0	1605.0	3.0	1.0
∞(HOPG)	1581.5	11.0	1.0	...	...	...

[a] Frequency at intensity maximum.
[b] Full width at half-maximum intensity (FWHM).
[c] Peak intensities are given in arbitrary units. For the stage $n = 4$ and 8 compounds, F_R gives the relative peak intensities.

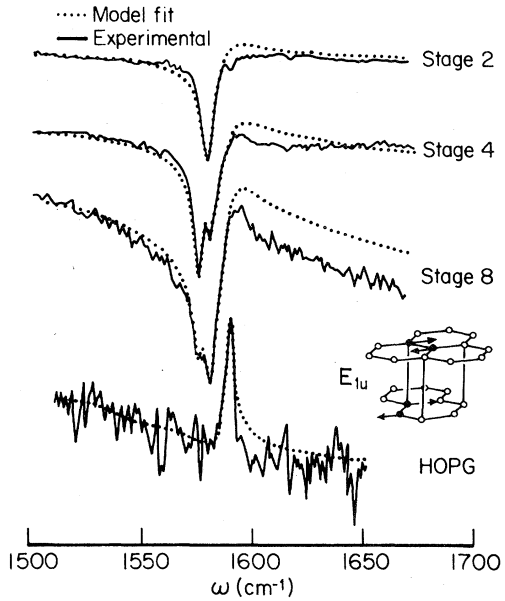

FIG. 4. Room temperature infrared reflectivity spectra from the c face for the energy range $1500 \leq \hbar\omega \leq 1650$ cm^{-1} for stage $n = 2, 4$, and 8 graphite-$AlCl_3$ and for pristine graphite (HOPG). No infrared structure was observed for stage-1 graphite-$AlCl_3$. Results for the model fit using the parameters listed in Table III are given by the dashed curves. The graphite E_{1u} mode is shown in the inset.

that can be identified with an in-plane $\hat{E}_{2g_2}$ mode. To extract the lattice mode frequency, linewidth, and oscillator strength, a line-shape analysis similar to the analysis described in Ref. 5 was performed and results for these parameters are given in Table III. The computed reflectivity using these parameters is shown in Fig. 4 by the dotted curves. It is significant that for the stage-1 compound, no infrared-active modes are found, in agreement with infrared measurements of the stage-1 alkali-metal donor compounds with K, Rb, and Cs.[24] Although this is the first report of the absence of infrared-active modes in acceptor compounds, we believe this absence to be a general phenomenon in acceptor compounds. For the case of the Br_2 acceptor compounds it has not been possible to produce a stage-1 compound, while for $FeCl_3$ intercalants it has not been possible to prepare a large, single-staged stage-1 sample, such as is required for infrared measurements. We attribute previous reports[11] of an infrared-active E_{1u}-like mode in stage-1 $FeCl_3$ to be due to an admixture of higher-stage material. In physical terms, a single graphite layer having 2 atoms/(unit cell) has an in-plane Raman-active optic E_{2g} mode and an acoustic E_{1u} mode corresponding to simple translation at $\vec{q} = 0$ ($\omega = 0$).

The analysis in Table III shows three infrared-active modes for compounds with stages $n = 2$, 4, and 8. For the stage $n = 4$ and 8 compounds, we identify the highest-frequency mode with the graphite interior layers because of its close proximity to the E^0_{1u} graphite mode and because it is not found in stages 1 and 2. We attribute the downshifted modes in stages $n = 2$, 4, and 8 to contributions from pairs of graphite layers containing a bounding graphite layer. This identification is supported by the rapid increase in intensity for the $\hat{E}_{1u}$ and E^*_{1u} modes with increasing $1/n$ as found in the data in Table III. This increase in intensity is more clearly delineated for the $\hat{E}_{1u}$ modes because of their smaller linewidths.

All results for the peak frequencies for the Raman (Fig. 3) and infrared (Fig. 4) spectra are summarized in Fig. 5, where the dependence on reciprocal stage ($1/n$) of the various mode frequencies is given. Also given in Fig. 5 are parameters for the slope and for the intercept at $1/n \to 0$, obtained from a least-squares fit. The two Raman-active modes for graphite-$AlCl_3$ show a similar upshift in frequency with $1/n$. This upshift is qualitatively similar to that in $FeCl_3$,[11] but the upshift is somewhat larger for $AlCl_3$ than

TABLE III. Parameters for infrared-active modes in graphite-$AlCl_3$.[a,b]

Stage	$\hat{E}_{1u}$ mode ω_0 (cm^{-1})	Γ (cm^{-1})	F_{ir}	E^*_{1u} mode ω_0 (cm^{-1})	Γ (cm^{-1})	F_{ir}	E^0_{1u} mode ω_0 (cm^{-1})	Γ (cm^{-1})	F_{ir}
1[c]	...			...			...		
2	1580.6	3.0	0.062	1584.0	8.0	0.120	...		
4	1576.8	2.4	0.020	1582.5	6.0	0.071	1588.0	10	0.048
8	1576.0	4.0	0.004	1583.0	7.8	0.030	1587.5	10	0.015

[a] For HOPG, there is one ir-active mode (E_{1u} symmetry) with parameters: frequency at peak intensity $\omega_0 = 1587.5$ cm^{-1}, FWHM intensity $\Gamma = 2$ cm^{-1}, and relative oscillator strength $F_{ir} = 0.006$ (Ref. 11).

[b] The ir spectra are analyzed by $\epsilon(\omega) = \epsilon_0 + \epsilon_{Drude} + \sum F_{ir}\,\omega_0^2/(\omega_0^2 - \omega^2 - i\Gamma\omega)$.

[c] No ir-active modes are observed for stage-1 graphite-$AlCl_3$.

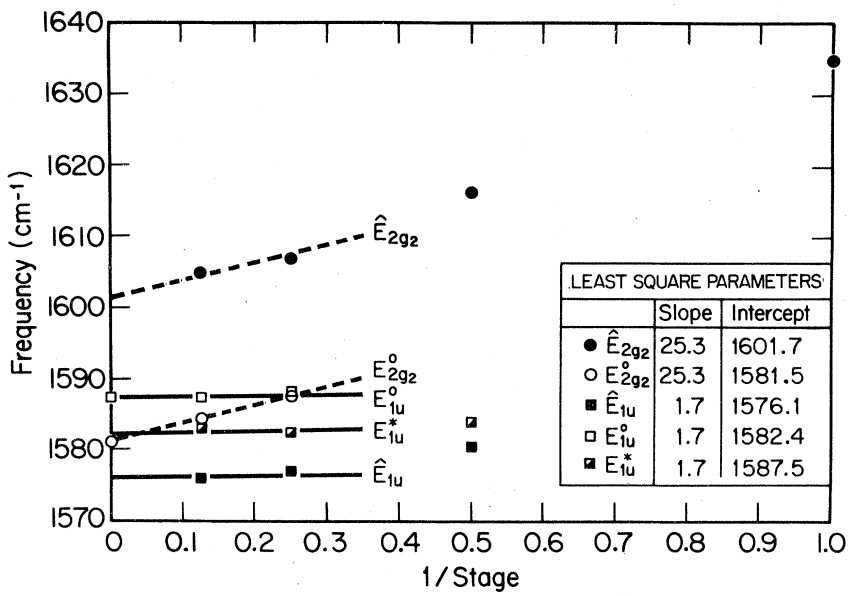

FIG. 5. The inverse stage ($1/n$) dependence of the mode frequencies for the Raman-active $\hat{E}_{2g_2}$, $E^0_{2g_2}$ modes and the infrared-active $\hat{E}_{1u}$, E^0_{1u}, E^*_{1u} modes. The dashed lines represent a least-squares fit for $n>3$ of both Raman-active modes (taken together). The solid lines represent a least-squares fit of the infrared-active modes taken together. Included in the inset are the least-squares parameters for the slope and $1/n \to 0$ intercept.

for $FeCl_3$ (slope is 25.3 for $AlCl_3$ and 9.5 for $FeCl_3$). For the graphite-$AlCl_3$ system, the Raman doublet separation between $\hat{E}_{2g_2}$ (bounding modes) and $E^0_{2g_2}$ (interior modes) is 20 ± 1 cm^{-1}. There seems to be little dependence of the infrared-active modes on $1/n$, in contrast with the results reported for $FeCl_3$.[11] One possible reason for this discrepancy may be due to the smaller number of samples used in the present analysis relative to the many samples that were measured and analyzed for the case of graphite-$FeCl_3$.[11] The frequency difference between the highest frequency mode (E^0_{1u}) and the intermediate frequency mode (E^*_{1u}) is 5 ± 1 cm^{-1} and the frequency difference between the intermediate (E^*_{1u}) and lowest ($\hat{E}_{1u}$) frequency modes is 6 ± 1 cm^{-1}. For comparison, the frequency difference between the E^0_{1u} and $\hat{E}_{1u}$ modes in graphite-$FeCl_3$ was found to be 4 ± 1 cm^{-1}, which is significantly smaller than for graphite-$AlCl_3$. On the other hand, the $(1/n)$-dependent frequency upshifts for the Raman modes found for graphite-$AlCl_3$ are consistent with the previously noted behavior for acceptor compounds; this behavior is to be contrasted with that in donor compounds where the $\hat{E}_{2g_2}$ and $E^0_{2g_2}$ modes both exhibit a $(1/n)$-dependent downshift in frequency.[8]

ACKNOWLEDGMENTS

The authors wish to thank Dr. A. W. Moore of Union Carbide for his generous contribution of HOPG material and Professor M. S. Dresselhaus for numerous discussions. The project was supported through ONR Grant No. N00014-77-C-0053. G. M. Gualberto was supported by FAPESP, Saõ Paulo, Brazil.

*Center for Materials Science and Engineering.
†Present address: Department of Physics, UNICAMP, Saõ Paulo, Brazil.
‡Department of Electrical Engineering and Computer Science.
§Francis Bitter National Magnet Laboratory, supported by NSF.

[1]R. Nicklow, N. Wakabayashi, and H. G. Smith, Phys. Rev. B 5, 4951 (1972).
[2]L. G. Brillson, E. Burstein, A. A. Maradudin, and T. Stark, in *Proceedings of the International Conference on the Physics of Semimetals and Narrow Gap Semiconductors, Dallas, Texas, 1970*, edited by D. L. Carter and R. T. Bate (Pergamon, New York, 1971), p. 187.
[3]F. Tuinstra and G. L. Koenig, J. Chem. Phys. 53, 1126 (1970); R. A. Friedel and G. C. Carlson, J. Phys. C 75, 1149 (1971).
[4]R. J. Nemanich, G. Lucovsky, and S. A. Solin, Solid State Commun. 23, 117 (1977).
[5]M. S. Dresselhaus and G. Dresselhaus, in *Physics and Chemistry of Materials with Layered Structures*, edited by F. Lévy (Reidel, Dordrecht, Holland), Vol. 5.

[6]M. S. Dresselhaus, G. Dresselhaus, P. C. Eklund, and D. D. L. Chung, Mater. Sci. Eng. 31, 141 (1977).
[7]R. G. Nemanich, S. A. Solin, and D. Guérard, Phys. Rev. B 16, 2965 (1977).
[8]S. A. Solin, Mater. Sci. Eng. 31, 153 (1977).
[9]J. J. Song, D. D. L. Chung, P. C. Eklund, and M. S. Dresselhaus, Solid State Commun. 20, 1111 (1976).
[10]P. C. Eklund, N. Kambe, G. Dresselhaus, and M. S. Dresselhaus, Phys. Rev. B 18, 7069 (1978).
[11]C. Underhill, S. Y. Leung, G. Dresselhaus, and M. S. Dresselhaus, Solid State Commun. 29, 769 (1979).
[12]Infrared structure associated with the intercalate layers has not yet been reported.
[13]S. A. Solin and R. J. Nemanich, Bull. Am. Phys. Soc. 20, 429 (1975).
[14]W. Metz and D. Holwein, Carbon 13, 87 (1975).
[15]W. Metz and L. Siemsglüss, Mater. Sci. Eng. 31, 119 (1977).
[16]G. Schoppen, L. Meyer-Spasche, L. Siemsglüss, and W. Metz, Mater. Sci. Eng. 31, 115 (1977).
[17]T. Sasa, Y. Takahashi, and T. Mukaibo, Carbon 9, 407 (1971).
[18]J. G. Hooley and M. Bartlett, Carbon 5, 417 (1967).
[19]J. G. Hooley and R. N. Soniassy, Carbon 8, 191 (1970).
[20]W. Rüdorff and R. Zeller, Z. Anorg. Allg. Chem. 279, 182 (1955).
[21]S. Y. Leung, C. Underhill, G. Dresselhaus, T. Krapchev, R. Ogilvie, and M. S. Dresselhaus, Solid State Commun. (to be published).
[22]S. Y. Leung, C. Underhill, G. Dresselhaus, T. Krapchev, R. Ogilvie, and M. S. Dresselhaus (unpublished).
[23]C. L. Lau and M. S. Dresselhaus, Phys. Rev. (to be published).
[24]S. Y. Leung, C. Underhill, G. Dresselhaus, and M. S. Dresselhaus (unpublished).